Appl Nanosci (2011) 1:13–18
DOI 10.1007/s13204-011-0002-7

ORIGINAL ARTICLE

Nanoscale microwave microscopy using shielded cantilever probes

Keji Lai · Worasom Kundhikanjana · Michael A. Kelly · Zhi-Xun Shen

Received: 7 March 2011 / Accepted: 9 March 2011 / Published online: 21 April 2011

Abstract Quantitative dielectric and conductivity mapping in the nanoscale is highly desirable for many research disciplines, but difficult to achieve through conventional transport or established microscopy techniques. Taking advantage of the micro-fabrication technology, we have developed cantilever-based near-field microwave probes with shielded structures. Sensitive microwave electronics and finite-element analysis modeling are also utilized for quantitative electrical imaging. The system is fully compatible with atomic force microscope platforms for convenient operation and easy integration of other modes and functions. The microscope is ideal for interdisciplinary research, with demonstrated examples in nano electronics, physics, material science, and biology.

Keywords Nanoscale imaging · Microwave microscopy · Quantitative dielectric mapping · MEMS cantilevers · Non-destructive sensing

Introduction

The understanding and manipulating of nanoscale electrical properties are of fundamental importance for novel materials and devices. In particular, the prosperity of modern information technology is deeply associated with the comprehensive knowledge of solid-state physics and the remarkable tunability of local conductivity in semiconductors. The new era of nanoscience and nanotechnology demands further breakthroughs in the investigation of exotic quantum materials and advanced device designs. It is therefore imperative to develop a full spectrum of scientific tools that perform direct electrical measurements in the microscopic length scale.

Most of the established microscopy instruments, such as optical microscope, scanning and transmission electron microscopes (SEM/TEM), and atomic force microscope (AFM), provide only the structural or topographic information of the samples. Various scanning probes are also developed to access the local electrical properties—scanning tunneling microscope (STM) for density of states, electrostatic force microscope (EFM) for surface potential, conductive AFM (C-AFM) for spreading resistance, and scanning gate microscope (SGM) for current path (Meyer et al. 2003). A missing element in the list is the collective dielectric response, which is critical for both scientific understandings and engineering solutions. The electrical interaction between the sample and the probe effectively modifies the tip impedance. In addition, the local conductivity and dielectric constant can be derived from the real and imaginary parts of this impedance. At DC or low frequency AC (MHz) fields, the impedance measurements usually require the patterning of counter electrodes and carefully prepared surface conditions. On the other hand, local dielectric imaging above THz frequencies, widely known as near-field scanning optical microscopy (NSOM) (Rosner and van der Weide 2002), primarily obtains optical (inter- or intra-band transitions) rather than quasi-static electrical information. The GHz microwave frequency regime is thus best suited for such purpose.

Near-field microwave microscopy has been an active research field in the past two decades (Rosner and van der

K. Lai (✉) · W. Kundhikanjana · M. A. Kelly · Z.-X. Shen
Department of Physics and Applied Physics,
Geballe Laboratory for Advanced Materials,
Stanford University, Stanford, CA 94305, USA
e-mail: kejilai@gmail.com

Weide 2002; Anlage et al. 2001; Anlage et al. 2006). Recent developments are focused on cantilever-based probes due to the compatibility with the state-of-the-art AFM platforms (Tabib-Azar and Wang 2004; Wang et al. 2007; Lai et al. 2007; Melikyana et al. 2009; Karbassi et al. 2008; Huber et al. 2010; Zhang et al. 2010). It is the goal of this article to review the basic principles, probes, and electronics of the AFM-compatible microwave impedance microscope (MIM) (Lai et al. 2007), as well as its applications in a broad range of disciplines. More comprehensive reviews of other configurations of the microwave probes are found in references (Rosner and van der Weide 2002; Anlage et al. 2001, 2006).

Experimental setup

Cantilever probe

Taking advantage of the high quality factors of microwave resonators, early implementations of microwave microscopes are configured as a sharp needle tip protruding from a cavity or transmission line resonator (Imtiaz and Anlage 2003; Kim et al. 2003; Gao et al. 1997; Wang et al. 2002). The system, as shown in Fig. 1a, is usually bulky and highly sensitive to temperature fluctuations. Special scanners are required and the tip apex easily gets blunted because of the lack of height control feedback. Microfabricated cantilever probes (Fig. 1b) on AFM platforms remove the above difficulties. They are mass produced on the wafer scale. Due to the mature MEMS technology, tip diameters below 100 nm are routinely achieved and well preserved over many scans because of the good feedback control. Current efforts are made toward the integration of MIM as a standard mode in AFM. Local properties from other AFM modes (STM, C-AFM, EFM, SGM, NSOM…) can then be collected simultaneously with the local dielectric information, with controlled external conditions, such as temperature, illumination, and liquid environment.

The stray field contribution from non-apex part of the cantilever probe presents a serious problem to this technique. Without careful shielding of the center conductor, significant topographic artifact will be mixed into the microwave signal. The schematic of our shielded cantilever tip (Lai et al. 2007, Lai et al. 2008a, b) is shown in Fig. 1c. The Al or Au center conductor, 10 μm in width, 1 μm in thickness, and 1 mm in length, is sandwiched between two silicon nitride (1–2 μm) layers. The dimensions are chosen so that the series resistance, background capacitance, and the mechanical property (spring constant $\sim$1 N/m) are optimized. We emphasize that heavily doped Si, although preferred from the micro-fabrication process, is too resistive for the center conductor and results in much weaker microwave signals. A thin (200 nm) metal layer covering the entire handle chip is connected to the ground of the feed line, providing RF shielding to the signal line. Most data in this paper were taken by tips shown in the SEM images in Fig. 1d, which were formed by depositing Pt in the focused-ion beam chamber (Lai et al. 2007, 2008). Our recent progress in MEMS would eventually eliminate this one-at-a-time process.

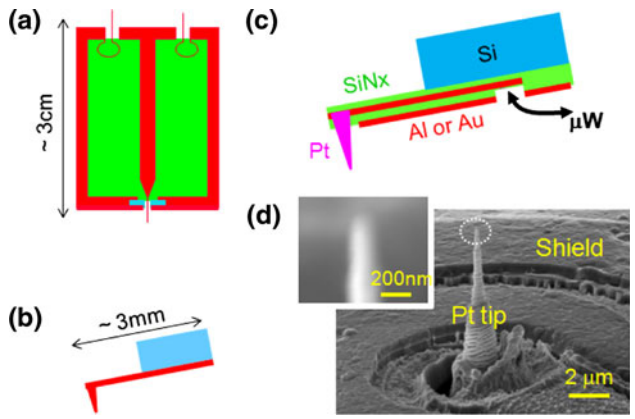

Fig. 1 **a** Schematic of microwave microscope based on a sharp needle extended from a cavity resonator, which is bulky and difficult to integrate with existing scanning platforms. **b** Schematic of an unshielded cantilever probe. **c** Layer structure of the shielded MEMS cantilever. The microwave signal is introduced through a bonding pad on the handle chip to the metal center conductor, which is sandwiched in the SiN_x lever and shielded by the ground plane. **d** SEM image at the tip end showing the ring-like shield and the Pt tip. The *inset* shows the zoom-in view of the apex

Electronics

The schematic of the microwave electronics is shown in Fig. 2 (Lai et al. 2007, 2008). For good power transfer, an impedance (Z) match section, using either lumped elements, stub tuning, or decoupling capacitor/inductor, is needed to route the tip capacitance, in our case $C_{tip} \sim 1$ pF, to 50 Ω in transmission lines. The 1 GHz microwave, 0.1–10 μW in power, is fed into the tip through a directional coupler. The cancellation signal is also coupled in to suppress the background reflected signal for the subsequent 60 dB RF gain stage. The amplified microwave signal is then demodulated through a quadrature mixer. With properly adjusted phase to the local oscillator port, the two DC output channels from the mixer correspond to the imaginary (or capacitive, MIM-C) and real (or resistive, MIM-R) components of the tip-sample impedance. Under a bandwidth of 1 kHz for normal scanning rate, the minimal detectable impedance change limited by thermal and shot noises is equivalent to $\sim$1 aF (10^{-18}F) capacitance in parallel with the tip.

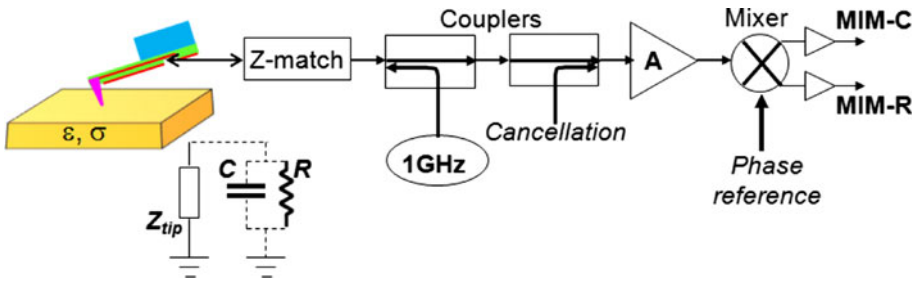

Fig. 2 Schematic of the detection electronics (detailed in the text). The *inset* shows the equivalent lumped-element circuit of the tip-sample interaction. The two MIM channels give DC signals proportional to changes of the tip-sample capacitance and reactance (inverse resistance), which can ultimately be converted to the local (ε, σ)

Simulation

Before discussing the experimental results, it is instructive to calculate the effective lumped elements, i.e., C and R in the inset of Fig. 2 induced by the tip-sample interaction. Although analytical solutions can be obtained after reasonable simplifications, it is much more accurate to perform numerical simulations to account for the actual tip-sample geometry (Lai et al. 2007, 2008). We utilize the commercial finite-element analysis (FEA) software COMSOL to directly compute the tip-sample admittance (inverse impedance). An example of the dense mesh created by COMSOL is given in the inset of Fig. 3a, where the tip shape and diameter of the apex (200 nm) agree with the SEM image in Fig. 1d. The sample is assumed to contain a thin film, 10-nm thickness, buried 30 nm below the surface. If the film is highly resistive $\rho > 10^2$ Ω cm, the entire sample appears as a good dielectric to the microwave probe and the signals in both channels are low. When the film is highly conductive $\rho < 10^{-3}$ Ω cm, it effectively becomes a ground plane that terminates all the electric fields. The tip-sample capacitance is now large and the effective resistance is again negligible. In between these two limits, there exists a phase-sensitive window, where the MIM-C signal increases with decreasing ρ and the MIM-R signal is non-monotonic. Both the simulation result (Fig. 3a) and the potential distribution (Fig. 3b) confirm such a response curve to the local conductivity. An interesting observation from Fig. 3b is that the spatial extension of quasi-static electric fields depends strongly on the local conductivity. In other words, although generally within the order of the apex diameter, the resolution of the microwave microscope varies with different samples.

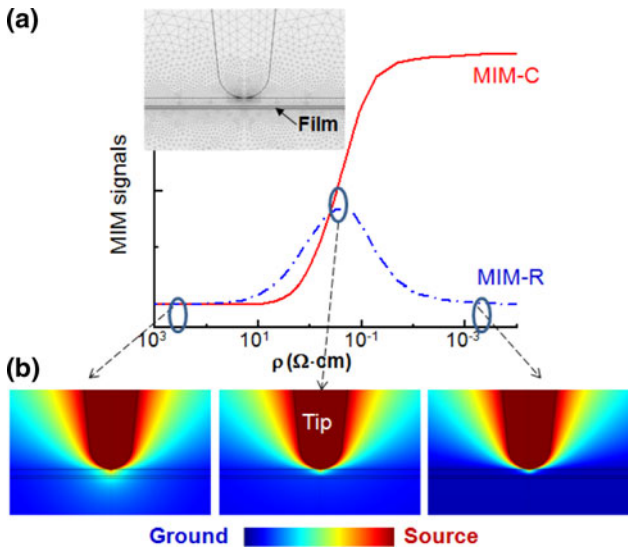

Fig. 3 **a** Finite-element analysis of a specific geometry (detailed in the text) in the *inset*, where the automatically generated mesh is shown. The MIM response to the local conductivity of the 10 nm film can be divided into three regimes. The corresponding quasi-static potential distributions are shown in **b**

Results and discussions

General-purpose electrical imaging

Because the MIM measurement is non-destructive and requires virtually no sample preparation, the tool is versatile to study problems from many scientific disciplines. A cryogenic version of the MIM is also implemented in our laboratory. Important results were obtained to understand the colossal magnetoresistive effect (Lai et al. 2010), metal–insulator transition in doped Si (Kundhikanjana et al. 2011), and quantum Hall edge states (Lai et al. 2011). We will focus on the room-temperature applications in this review.

In Fig. 4a, the high conductivity of ultra-thin Bi_2Se_3 nano-flakes is readily seen (Hong et al. 2010). In addition, a careful study further yields the relation between the conductivity and the layer thickness. The material is recently identified as topological insulators, a topic under extensive investigation in the condensed matter physics community. Two In_2Se_3 nano-ribbons are imaged in Fig. 4b (Lai et al. 2009). The zig-zag one on the bottom left appears darker than the SiN_x/Si substrate, indicating insulating phase here.

Interestingly, the straight ribbon on the top right clearly contains two domains—the bright conducting (crystalline) and dark insulating (amorphous) phases. Indeed, In_2Se_3 is known as a prototypical phase-change material for memory applications. In Fig. 4c, several chemically exfoliated graphene flakes on the SiO_2/Si wafer are observed (Kundhikanjana et al. 2009). The chemical process leaves appreciable amount of defects in the graphene, resulting in lower conductivity than the pristine sample peeled off from graphite. Both the local electrical defects and variation of conductivity from piece to piece are vividly demonstrated by the MIM data. The microwave frequency is a particularly important regime for biological research because of the high sensitivity to water and mineral content in tissues (Lai et al. 2007). We show an image of the cells and Ommatidial clusters of the fruit fly (*Drosophila*) compound eyes in Fig. 4d. At the moment, the imaging is performed using dried samples and we are working actively toward in vitro studies.

The sensitivity to local electrical properties makes the microwave probe an effective sensor for photoconductivity. As schematically shown in Fig. 4e, a layer of 50 nm Al_2O_3 was deposited on an intrinsic Si wafer and patterned into parallel stripes. Without light, the contrast is only in the MIM-C channel (not shown) and the MIM-R image is featureless. The intrinsic Si becomes very lossy with illumination above the band gap and appears much brighter than the region covered by Al_2O_3, which acts as a series capacitor, in the MIM-R channel. Future work with controlled light intensity and wavelength is expected to yield more quantitative information and such capability of the microwave probe can be utilized in the search of energy conversion materials, as well as characterization of the solar cells.

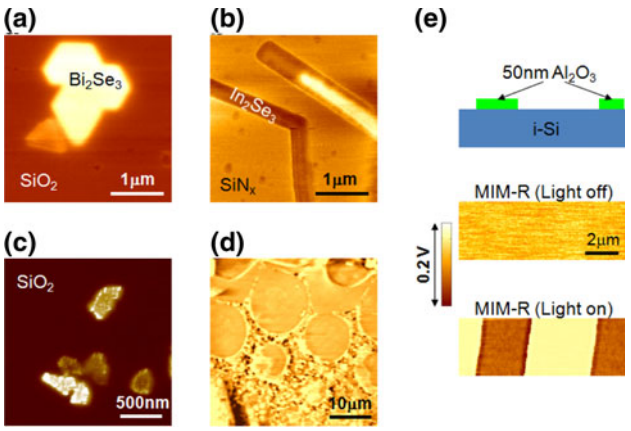

Fig. 4 **a–d** MIM-C images of various samples described in the main text, demonstrating the versatility of the technique. **e** Schematic (*top*) of the sample, in which Al_2O_3 stripes are patterned on intrinsic Si wafer, showing photoconductivity effect. The MIM-R image is featureless when external illumination is turned off (*middle*) and shows clear contrast (*bottom*) when light is on

Quantitative microwave microscopy

The FEA simulation introduced above allows one to obtain quantitative information of the sample. Figure 5a shows a set of MIM-C images of a selectively doped Si sample, on which various thickness of Al_2O_3 films were subsequently deposited. The contrast between the doped and intrinsic regions decreases as increasing Al_2O_3 thickness. We note that the contrast is clearly discerned for features 300 nm below the surface, which demonstrates the ability of subsurface imaging by MIM. In the FEA modeling, standard or measured sample parameters are used—tip diameter 200 nm, native oxide thickness 1.5 nm, $\varepsilon_r(SiO_2)$–4, $\varepsilon_r(Al_2O_3)$–10, $\varepsilon_r(Si)$–12, $\rho(\text{n-Si}) = 0.5\ \Omega\ \text{cm} \ll \rho(\text{i-Si})$. The electronics amplify 1aF impedance change to 10 mV in the MIM-C output. As shown in Fig. 5a, the fit of the simulated curve to the experimental data is excellent.

Figure 5b provides another example for quantitative microwave imaging analysis (Lai et al. 2008). The n-type ion-implantation resulting in doping level of 2×10^{16} cm^{-3} at selected surface regions (dots in the images) was performed on four wafers—Si-HR (almost intrinsic), Si-L (p-type, 6×10^{14} cm^{-3}), Si–K (p-type, 1×10^{15} cm^{-3}), and Si–I (p-type, 4×10^{16} cm^{-3}). The MIM-C images reveal clear conductivity difference between the implanted dots and the un-implanted background, strongest in Si-HR and weakest in Si–I. In fact, since the implanted level is below the substrate concentration in Si–I, the contrast of the dots over the background is reversed here compared with other wafers. Using again measured parameters for simulation, we obtain very good agreement between modeling and the experiment.

Tapping mode MIM

The results discussed so far were taken in the contact mode and such an operation is susceptible to tip wearing and sample damage. More importantly, thermal or other electronic drifts are usually observed in the microwave images for long scans. The tapping mode AFM operation, where the cantilever vibrates at its mechanical resonant frequency above the sample surface, effectively removes these problems. In this mode, the tapping introduces a time-dependent capacitor (air, $\varepsilon_r = 1$) in series with the sample impedance and the MIM signals are modulated at the same frequency, in our case $\sim$150 kHz, and detected by lock-in amplifiers. Through the FEA analysis, quantitative sample information is again obtained. In Fig. 6a, we show the lock-in signals on a number of high-quality SiO_2 or Si_3N_4 thin films deposited on p-Si wafers (Lai et al. 2009). The ability to perform

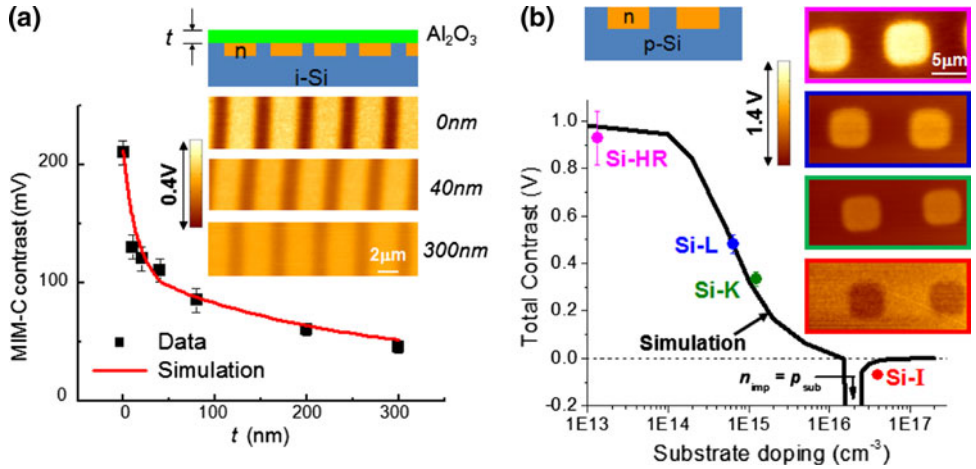

Fig. 5 **a** MIM-C contrast between the implanted and un-implanted regions (sample structure shown in the *inset*) as a function of the Al_2O_3 over-layer thickness t. The *red solid line* is a fit to the experimental data using the FEA simulation. Three representative MIM-C images with $t = 0$, 40, and 300 nm are shown in the inset. **b** Contrast between the n-type implanted region and the p-type wafer (*inset top left*) versus the substrate doping level. The FEA result is plotted as the *black solid line*. MIM-C images on Si-HR (*purple*), Si-L (*blue*), Si–K (*green*), and Si–I (*red*) samples are shown in the *inset*. The good agreements between data and simulation in both **a** and **b** demonstrate the ability of quantitative electrical imaging

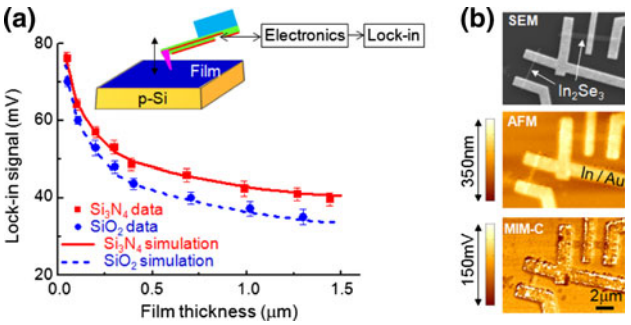

Fig. 6 **a** Tapping mode MIM-C signals as a function of the SiO_2 and Si_3N_4 film thickness. Schematic of the tapping mode setup is shown in the *inset*. **b** SEM, AFM, and tapping mode MIM-C images of two In_2Se_3 nano-ribbons contacted by In/Au electrodes. The ribbon on the *bottom left* is more conducting (*brighter*) than the one on the top right (*darker*)

absolute dielectric constant measurement can be appreciated from the excellent fitting of data to the simulation curves. In Fig. 6b, the SEM, AFM, and tapping mode MIM-C images of In_2Se_3 nano-ribbons contacted by In/Au electrodes are depicted. The ribbon on the bottom left appears brighter than the one on the top right, consistent with the lower resistance of the former ($\sim$kΩ) than the latter ($\sim$GΩ) one. We emphasize that, unlike most contact mode images, the tapping mode images do not require the removal of a slow drift background. On the other hand, since the non-contact tip-sample interaction is dominated by the air capacitor, the MIM-R channel output using conventional lock-in detection is dramatically suppressed. We are currently working on different electronic schemes to regain the full impedance information in the tapping mode.

Summary and outlook

The successful implementation of the microwave impedance microscope benefits from innovations in micromachined shielded probes, ultra-sensitive microwave electronics, advanced finite-element modeling, and the adaption to AFM platforms. The microwave imaging requires little sample preparation and is non-destructive. The ability to perform quantitative dielectric and conductivity mapping in the 100-nm length scale has found multidisciplinary applications in electrical engineering, physics, material science, chemistry, and biology.

Active research is under way to further improve the technique. The next generation cantilever probes would simultaneously fulfill the following requirements: sharp—10–20 nm diameter, shielded—coaxial structure all the way to the apex, scalable—wafer scale batch process, strong—rugged metal at the apex, and sensitive—small series resistance and background capacitance. The microwave electronics will become broadband and cover several orders of magnitude from 50 MHz to 20 GHz. Sophisticated 3D FEA simulation will be explored to enable quantitative mapping of (ε, σ) on samples with arbitrary shapes. Finally, the combination of AFM and MIM has provided us a wonderful platform to simultaneously collect the mechanical, electrical, magnetic, static or temporal information under various conditions. What we have seen is only the tip of the iceberg, with tremendous research opportunities in the future.

Acknowledgments This work is supported by Award No. KUS-F1-033-02, made by King Abdullah University of Science and

Technology (KAUST) under the global research partnership (GRP) program. Additional supports are from Center of Probing the Nanoscale (CPN), Stanford University, a gift grant of Agilent Technologies, Inc., NSF Grant DMR-0906027, and DOE under Contract Nos. DE-FG03-01ER45929-A001 and DE-FG36-08GOI8004. CPN is an NSF NSEC, NSF Grant No. PHY-0425897.

References

Anlage SM, Steinhauer DE, Feenstra BJ, Vlahacos CP, Wellstood FC (2001) In: Weinstock H, Nisenoff M (eds) Microwave superconductivity. Kluwer, Amsterdam

Anlage SM, Talanov VV, Schwartz AR (2006) In: Kalinin SV, Gruverman A (eds) Scanning probe microscopy: electrical and electromechanical phenomena at the nanoscale. Springer, New York

Gao C, Wei T, Duewer F, Lu Y, Xiang X-D (1997) High spatial resolution quantitative microwave impedance microscopy by a scanning tip microwave near-field microscope. Appl Phys Lett 71:1872

Hong SS, Kundhikanjana W, Cha J, Lai K, Kong D, Meister S, Kelly MA, Shen ZX, Cui Y (2010) Ultrathin topological insulator Bi_2Se_3 nanoribbons exfoliated by atomic force microscopy. Nano Lett 10:3118

Huber HP, Moertelmaier M, Wallis TM, Chiang CJ, Hochleitner M, Imtiaz A, Oh YJ, Schilcher K, Dieudonne M, Smoliner J, Hinterdorfer P, Rosner SJ, Tanbakuchi H, Kabos P, Kienberger F (2010) Calibrated nanoscale capacitance measurements using a scanning microwave microscope. Rev Sci Instrum 81:113701

Imtiaz A, Anlage SM (2003) A novel STM-assisted microwave microscope with capacitance and loss imaging capability. Ultramicroscopy 94:209

Karbassi A, Ruf D, Bettermann AD, Paulson CA, van der Weide DW, Tanbakuchi H, Stancliff R (2008) Quantitative scanning near-field microwave microscopy for thin film dielectric constant measurement. Rev Sci Instrum 79:094706

Kim J, Lee K, Friedman B, Cha D (2003) Near-field scanning microwave microscope using a dielectric resonator. Appl Phys Lett 83:1032

Kundhikanjana W, Lai K, Wang H, Dai H, Kelly MA, Shen ZX (2009) Hierarchy of electronic properties of chemically derived and pristine graphene probed by microwave imaging. Nano Lett 9:3762

Kundhikanjana W, Lai K, Kelly MA, Shen ZX (2011) Cryogenic microwave imaging of metal–insulator transition in doped silicon. Rev Sci Instrum (in press)

Lai K, Ji MB, Leindecker N, Kelly MA, Shen ZX (2007) Atomic-force-microscope-compatible near-field scanning microwave microscope with separated excitation and sensing probes. Rev Sci Instrum 78:063702

Lai K, Kundhikanjana W, Kelly MA, Shen ZX (2008a) Modeling and characterization of a cantilever-based near-field scanning microwave impedance microscope. Rev Sci Instrum 79:063703

Lai K, Kundhikanjana W, Kelly MA, Shen ZX (2008b) Calibration of shielded microwave probes using bulk dielectrics. Appl Phys Lett 93:123105

Lai K, Peng H, Kundhikanjana W, Schoen DT, Xie C, Meister S, Cui Y, Kelly MA, Shen ZX (2009a) Nanoscale electronic inhomogeneity in In_2Se_3 nanoribbons revealed by microwave impedance microscopy. Nano Lett 9:1265

Lai K, Kundhikanjana W, Peng H, Cui Y, Kelly MA, Shen ZX (2009b) Tapping mode microwave impedance microscopy. Rev Sci Instrum 80:043707

Lai K, Kundhikanjana W, Nakamura M, Kawasaki M, Tokura Y, Kelly MA, Shen ZX (2010) Mesoscopic percolating resistance network in a strained manganite thin film. Science 329:190

Lai K, Kundhikanjana W, Shabani J, Shayegan M, Kelly MA, Shen ZX (2011) Coulomb driven quantum Hall edge strips (in review)

Melikyana H, Sargsyana T, Babajanyana A, Kima S, Kima J, Leea K, Friedman B (2009) Hard disk magnetic domain nano-spatial resolution imaging by using a near-field scanning microwave microscope with an AFM probe tip. J Magn Magn Mater 321:2483

Meyer E, Hug HJ, Bennewitz R (2003) For a review of various scanning probe modes on AFM, see Scanning probe microscopy: the lab on a tip. Springer, Berlin

Rosner BT, van der Weide DW (2002) High-frequency near-field microscopy. Rev Sci Instrum 73:2505

Tabib-Azar M, Wang Y (2004) Design and fabrication of scanning near-field microwave probes compatible with atomic force microscopy to image embedded nanostructures. IEEE Trans Microwave Theory Tech 52:971

Wang Z, Kelly MA, Shen Z-X, Wang G, Xiang X-D, Wetzel JT (2002) Evanescent microwave probe measurement of low-k dielectric films. J Appl Phys 92:808

Wang Y, Bettermann AD, van der Weide DW (2007) Process for scanning near-field microwave microscope probes with integrated ultratall coaxial tips. J Vac Sci Technol B 25:813

Zhang L, Ju Y, Hosoi A, Fujimoto A (2010) Microwave atomic force microscopy imaging for nanometer-scale electrical property characterization. Rev Sci Instrum 81:123708